

Novel micromachined lumped band pass filter for 5.2 GHz WLAN applications

Andrei A. Muller¹, Dan Neculoiu², Alina Cismaru¹, Patrik Pons³, Robert Plana³, Dan Dascalu¹
and Alexandru Muller¹

¹IMT-Bucharest, 32B Erou Iancu Nicolae street, R-07719, Bucharest, Romania

²Politehnica Univ. Bucharest, Electronics Dept, 313 Splaiul Independentei, R060042, Romania

³LAAS-CNRS Toulouse, 7, Av. Colonel Roche, 31077 Toulouse, Cedex 4, France

Correspondence address (Alexandru Muller) alexandru.muller@imt.ro, Phone : +40 21 2690775,
Fax : +40 21 2690772

Abstract

This paper describes the design, manufacturing and experiments of a lumped element band pass filter in a new topology. The design starts from a second order capacitive coupled resonator topology. An additional series inductor is inserted in the filter classical topology, for shifting two transmission zeros on the real frequency axes in the filter's band stop, to improve the high frequency response. Design equations for the new band stop resonance frequency are presented together with the analysis of the correspondence between the band pass and band stop attenuation vs. the quality factor of the shunt and series inductors used. The filter is supported on a 6.4 μm thin dielectric membrane, and is manufactured using silicon micromachining, in CPW technology. Measurements illustrated a minimum 2.75 dB insertion loss at 5.5 GHz in the band pass, and more than 40 dB attenuation, at 8 GHz.

Keywords: Band pass filter, inductors, lumped elements, micromachining, WLAN

1. Introduction

Wireless communications have developed rapidly in the last years and have been applied for many services such as Internet and mobile phones. Band pass filters are important components of wireless systems as they enable band selection in RF transceivers. The growing wireless market has raised interest in novel architecture design and new technologies in order to reduce complexity and increase the performances.

Different kind filters for wireless applications in the 5 GHz frequency range with low insertion losses in the band pass have been reported in several technologies [1-5]. Lumped element filter design for this frequency range has been reported using low-temperature co-fired ceramic (LTCC) [6] or micromachining techniques [7]). MEMS technologies, including membrane suspended techniques, have been developed in the last years, with a lot of applications in manufacturing of circuits working in the microwave and millimeter wave frequency range [8-16]. The aim of this paper is to illustrate a new topology of a lumped element band pass filter with an improved high frequency band stop response. Analyzing the transfer functions of the lumped topologies presented in [6] and [7] we found out that the transmission zeros of the presented WLAN filters, were at frequencies $f=0$ and $f=\infty$.

In this work, starting from a standard filter topology with transmission zeros at frequencies $f=0$ and $f=\infty$, we designed and fabricated a filter with improved frequency response by shifting a part from the zeros from $f=0$ to the real frequency axis, above the filter's band pass, for enhanced upper band stop rejection.

The novel filter's topology imposes a simple way to determine and shift the band stop resonance frequency compared to the typical filters that provide zeros in the band stop. The equations of the new filter topology show a band stop resonance determined by only 2 elements compared to the standard filter topologies where the band stop resonance is influenced by more filter elements.

The filter has two shunt inductors and one series inductor responsible for the transmission zero control. Next section briefly presents the design approach. The influence of the series and shunt inductors quality factors on the filter frequency response is investigated in detail for minimum insertion losses at 5.2 GHz (band pass) and maximum attenuation at 8 GHz (stop band).

Section 3 presents the filter fabrication and measurements. In order to increase the inductor quality factor, the structure was manufactured on a 6.4 μm thin $\text{SiO}_2/\text{Si}_{3.4}\text{N}_4/\text{SiO}_{0.7}\text{N}_{0.7}$ membrane. The membrane was released by silicon micromachining. The filter structures were measured on wafer and the results are in good agreement with electromagnetic simulations.

2. Filter design

The band pass filter structures are in coplanar waveguide (CPW) technology. The main steps of the design procedure are presented below. First the membrane supported lumped elements (spiral inductors and interdigital capacitors) are modelled using intensive electromagnetic (EM) simulations and a database was created [12, 13]. Next the filter prototype was investigated using the Ansoft Designer SV software package. The preliminary design consisted of a trade between the filter frequency response shapes and the available component values from the database. This investigation demonstrated the difficulty of the control for a given rejection frequency in the higher stop band. In order to solve this problem, the filter transfer response was investigated in deep on the basis of closed form equations and Mathematica software package. More details are given in this section.

Next step in the design flow is the filter layout generation and preliminary EM analyses with Zeland IE3D software package [17]. The simulator is based on the Method of Moments algorithm and performs electromagnetic analysis for arbitrary 3-D geometry maintaining full

accuracy at all frequencies. Because of the frequency dispersion of the lumped components parameters, the results differ from the prototype frequency response. Layout optimization started with the results from previous step as the initial guess. The IE3D software includes an optimisation engine that allows the definition of multiple objective functions. The optimised variables are the layout dimensions. The optimisation efficiency depends on how far is the initial guess from the desired filter response.

The design starts from the second order capacitive coupled resonator shown in Fig. 1. The filter transmission parameter $S_{21}(s)$ is derived in (1).

$$S_{21}(s) = \frac{2 * C_1^2 C_2 L_3^2 Z_0 * s^5}{P_1(s^6)} \quad (1)$$

where C_1, C_2 are the series capacitors, L_3 shunt inductors C_3 shunt capacitors, Z_0 the port impedance while s the complex frequency and $P_1(s^6)$ a polynomial of degree 6 in variable s . From (1) results that this topology causes five zeros at $\omega=0$ and one zero at $\omega=\infty$.

A simple way to obtain transmission zeros in the stop band for a band pass filter excepting the zeros in the origin and at infinity is to employ the topology presented in Fig. 2, mainly used for elliptical filter designs.

The transmission parameter of this filter can be expressed as (2).

$$S_{21}(s) = \frac{2C_1^2 C_2 Z_0 * s * \left(1 + s^2(L_3 C_3 + L_4 C_4 + L_4 C_3) + C_3 C_4 L_3 L_4 * s^4\right)^2}{P_2(s^6)} \quad (2)$$

where C_1, C_2 are the series capacitors, L_1, L_2 are the series inductors L_3, L_4, C_3, C_4 are the inductors, respectively capacitors from the ground branches from Fig.2 while $P_2(s^6)$ is

polynomial of degree 6 in s . This topology generates zeros in the stop band their position being determined by the values of 4 different elements (L_3 , L_4 , C_3 , and C_4).

Our aim is to shift some zeros on the real frequency axes starting from the topology showed in Fig. 1 in order to obtain an improved stop band rejection. The aim is to have a transmission zero in the upper stopband (other than the zero at infinity). The position of this resonance frequency should be easier controlled. The purpose was to do this without to increase too much the filter's complexity from Fig.1 and also to obtain an easier way in controlling the band stop resonance compared to the simplest filter topologies that have band stop resonances as the filter in Fig. 2.

Generally this can be done perturbing the elements in the filter's topology without increasing the total number of the filter's zeros [11]. By inserting an additional inductor in parallel with C_2 from Fig.1 we obtain the topology in Fig. 3.

The new filter topology from Fig. 3 still has 6 zeros as the filter from Fig.1, the main difference is in the fact that two zeros move from $f=0$ on the real frequency axis, their position being imposed only by the resonance between C_2 and L_2 as shown below:

$$S_{21}(s) = \frac{2 * C_1^2 L_3^2 Z_0 * s^3 * (1 + C_2 L_2 s^2)}{P_3(s^6)} \quad (3)$$

where C_1 , C_2 , C_3 , L_1 , L_2 , Z_0 are the capacitors, inductors and port impedances from Fig. 3 and $P_3(s^6)$ a polynomial of degree 6 in s . Comparing (3) with (2) it may be seen that the transmission zero generated with (3) leads to frequency that can be shifted just by changing the values of L_2 and C_2 . Both (3) and (2) have besides the zeros at $\omega=0$ and $\omega=\infty$ other transmission zeros given by the numerator. Since the goal of the proposed filter is to have a high rejection level close to the pass band (3) gives a simple way to fine-tune the frequency corresponding to the additional transmission zero.

The effects of the additional series inductor (Fig.3) on the final filter's transmission parameter are evidenced by computing the insertion losses at 5.2 GHz for different values of the inductors quality factors. In Fig. 4 the insertion losses of the new filter as a function of inductors quality factors is presented. The series inductor quality factor has a much lower influence on the band pass insertion losses, a high shunt inductor quality factor would assure low losses in the band pass. The additional inductor's (L_2) effects in the filter's configuration, the band stop maximum attenuation is computed in respect to the series and shunt inductors, the dependence being presented in Fig. 5. It is observed that the rejection attenuation is practically determined only by the series inductor quality factor.

The LC components values in Fig. 3 are: $C_1=0.16$ pF, $C_2=0.06$ pF, $C_3=0.07$ pF, $L_2=6.8$ nH and $L_3=4.56$ nH if we want to fulfill requirements of the WLAN 5200 standard of ETSI (European Telecommunications Standard Institute). The values of the capacitors are low due the fact that the membrane on which the filter is suspended allows low values of capacitances and inductors with high quality factor.

A comparison between the filter's performances using the new topology presented in Fig. 3 and a filter without the additional inductor (the topology presented in Fig 1) is shown in Fig. 6. The values for the filter elements in Fig 1 are chosen so that the two topologies should generate the same pass band response ($C_1=0.27$ pF, $C_2=0.11$ pF, $C_3=0.26$ pF, $L_3=1.44$ nH). Fig. 6 outlines the benefit of the new topology presented in Fig 3. This topology generates a higher rejection level, close to the pass band, at higher frequencies.

In the design rules the metallization is considered gold 3 μm thick and the minimum distance between the capacitors digits is 10 μm . The filter layout was generated and optimized using Zeland IE3D. The final filter layout has 5.6 mm*3.7 mm.

3. Fabrication and measurements

For the filter manufacturing high resistivity ($\rho > 2 \text{ k}\Omega\text{cm}$), $\langle 100 \rangle$ oriented silicon wafers have been used. The wafer thickness was $400 \mu\text{m}$. A three layer membrane structure with a total thickness of $6.4 \mu\text{m}$ was deposited on the top of the wafer. The membrane structure was composed by the following layers: thermal SiO_2 ($0.8\mu\text{m}$), Low Pressure Chemical Vapor Deposition (LPCVD) $\text{Si}_{3.4}\text{N}_4$ ($0.6\mu\text{m}$) and LPCVD $\text{SiO}_{0.7}\text{N}_{0.7}$ ($5\mu\text{m}$). On the back side of the wafer there were deposited just first two layers (thermal SiO_2 and $\text{Si}_{3.4}\text{N}_4$), which will be used as mask for the membrane manufacturing, by a bulk micromachining process. A seed layer (Ti/Au $0.25\mu\text{m}$ thin) was deposited on the top of the wafer and then the filter structure patterned and manufactured by selective gold electroplating through the photo resist mask. The total thickness of the gold layer was about $2.5\mu\text{m}$. The next step was the partial silicon etching – first the dielectric layers were removed from the etching windows by Reactive Ion Etching (RIE) and after that, by using a DRIE (Deep RIE) process, silicon wafers were etched to remain $50\mu\text{m}$ bulk silicon under the membrane layers. The air bridges for the inductors were manufactured using standard procedures. A sacrificial layer (photoresist with a thickness of about $3\mu\text{m}$) was deposited and patterned. After the seed layer deposition ($0.05\mu\text{m}$ Au), bridges were obtained by gold electroplating up to the desired thickness ($\sim 2\mu\text{m}$) and etching through the resist mask. After sacrificial layer removing, the final structure was obtained by etching of the remaining bulk silicon under the membranes, using again a DRIE process. The top and bottom SEM photos of the filters are presented in Fig. 7a and Fig. 7b. The metallization layout of the filter components is visible through the transparent dielectric membrane. Air bridges were used to equalize the CPW grounds potential at the discontinuities. The shunt connected parallel LC resonant circuits from Fig.3 were split on both size of the CPW to obtain a compact structure.

S parameters measurements were performed using an on wafer measuring set-up equipped with Cascade Microtech coplanar probes and a vector Network Analyzer. The comparison

between the simulated using Zeland IE3D and the measured S parameters is presented in Fig. 8. The simulations are in good agreement with the measured results. The minimum pass band attenuation was 2.75 dB at 5.5 GHz and the rejection of -42 dB at 8 GHz. This demonstrates the concordance between the analytical approach (3), Zeland EM simulations and the high quality of the micromachining fabrication process. The results obtained for the rejection level, close to the pass band, are (according to our knowledge) the best results reported up to now for L, C filters operating in this frequency range.

4. Conclusions

A new lumped element micromachined band pass filter for WLAN 5200 standard was designed and manufactured. The measured results show a minimum 2.75 dB pass band attenuation at 5.5 GHz while achieving more than 40 dB attenuation at 8 GHz, which is higher than at the previous lumped element attenuations obtained in the upper band stop for WLAN filters. The band pass insertion losses are mainly due to the manufacturing problems. The benefits of an additional high quality series inductor in a classical topology are evident for improving the upper band stop attenuation of the filter.

References

- [1]. Chen C.Y, Hsu C.Y., Chuang H.R. Design of miniature planar dual – band filter using dual feeding structures and embedded resonator. *IEEE Microwave and Wireless Components Letters*, 2006;16:669 - 71
- [2] Chen C.Y., Hsu C.Y., A simple and effective method for microstrip dual – band filters design. *IEEE Microwave and Wireless Components Letters*, 2006;16:246 –8

- [3] Pallazari V, Pinel S, Laskar J, Roselli L, Tentzeris M. Design of an Asymmetrical Dualband WLAN Filter in Liquid Crystal Polymer System-On-Package Technology. IEEE Microwave and Wireless Components Letters, 2005;15:165-7
- [4] Bairavasubramanian R, Pinel S, Papapolymerou J., Laskar J., Quendo C, Rius E., et al. Dual-Band Filters for WLAN Applications on Liquid Crystal Polymer Technology, IEEE MTT-S International Digest 2005. p 533-6
- [5] Liao CK and Chang CY. Modified Parallel-Coupled Filter With Two Independently Controllable Upper Band stop Transmission Zeros. IEEE Microwave and Wireless Components Letters 2005;15:841-3
- [6] Joshi H. Chappel W. Dual band lumped – element band pass filter. IEEE Transactions on Microwave Theory and Techniques, 2006;54:4169 - 77
- [7] Kim J. M, Lee S, Park J. H., Kim J. M., Baek C.W., Kwon Y, et al. Digitally frequency – controllable dual – band WLAN filters using micromachined frequency – tuning elements. Proceedings of IEEE MEMS Conference, Istanbul, 2006. p. 158-61
- [8] Rebeiz G.M. RF MEMS theory, design and technology. John Wiley&sons, 2004
- [9] De Los Santos H. J. RF MEMS circuit design for wireless communications. Artech House, 2002
- [10] Iniewski K (editor). Wireless technology: Circuits systems and devices, chapter 22, CRC Press Taylor & Francis Group. 2007
- [11] Wenzel R. J. Understanding transmission zero movement in cross-coupled filters, IEEE MTT-S International Microwave Symposium digest, 2003. p 1459-62
- [12] Muller A. A., Neculoiu D., Vasilache D., Takacs A. Cismaru A. Lumped element bandpass micromachined filter for DCS 1800 filter applications, Proceedings of the IEEE Mediteranean Electrotechn.Conf. “Melecon 2006”, Malaga, 2006. p 643-6

- [13] Horng T.S., Peng K. C., Tsai J. K.. S parameter Formulation of Quality Factor for a Spiral Inductor generalized Two-Port Configuration. IEEE Transactions on Microwave Theory and Techniques, 2003;51:2 197-203,
- [14] Jhaa K. R, Raib M. A slow wave structure and its application in band pass filter design, Int. J. Electron. Commun. (AEÜ) 2010;64:p177–85
- [15] Pantazis A, Neculoiu D, Hazoupulos Z, Vasilache D, Lagadas M, Muller AA, et al. Millimeter wave passive circuits elements based on GaAs micromachining, Journal of Micromechanics and Microengineering 2005;15:p.S53-9.
- [16] Takacs A., Neculoiu D., Vasilache D., Muller A., Pons P. et al. Tunable bandstop MEMS filter for millimetre-wave applications, Electronics Letters 2007;43: p. 676-7.
- [17] IE3D User's Manual, 11, Zeland Software Inc., Fremont, CA, 2006

List of Figure captions

Fig. 1. Classical filter topology with transmission zeros at $\omega=0$, $\omega=\infty$

Fig. 2. Topology used essentially for elliptical filters

Fig. 3. Proposed new filter topology

Fig. 4. Insertion losses at 5.2 GHz vs. the series and shunt inductors quality factors respectively

Fig. 5. Maximum band stop insertion loss (rejection) vs. the series and shunt inductors quality factors respectively

Fig. 6 Magnitude of S_{21} for classical and new topology vs. frequency (simulated results)

Fig. 7 SEM photo of the filter structure: top view (a) and bottom view (b) the filter structure is visible through the transparent dielectric membrane

Fig. 8. Simulated and measured parameters of the structure

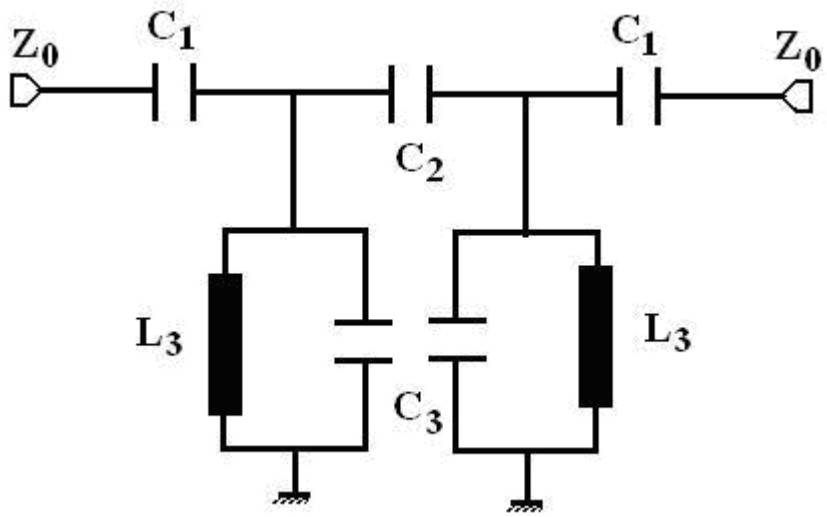


Fig 1

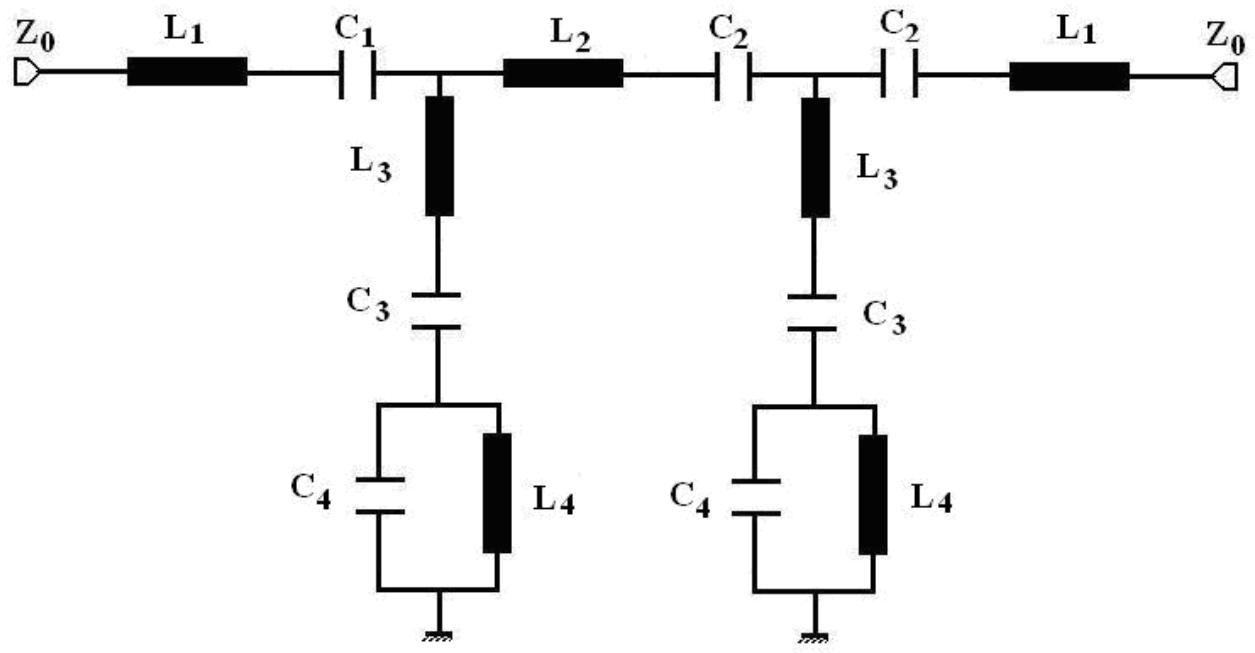


Fig.2

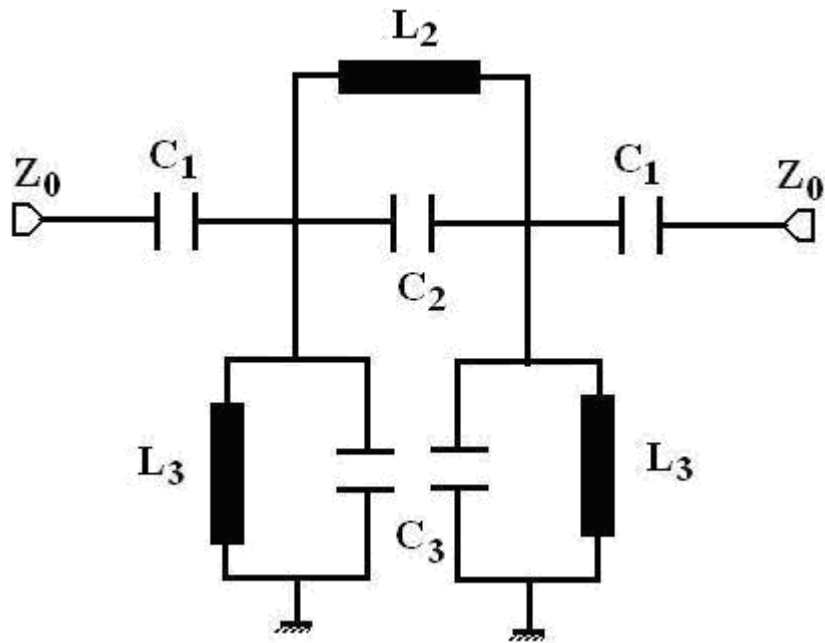


Fig.3

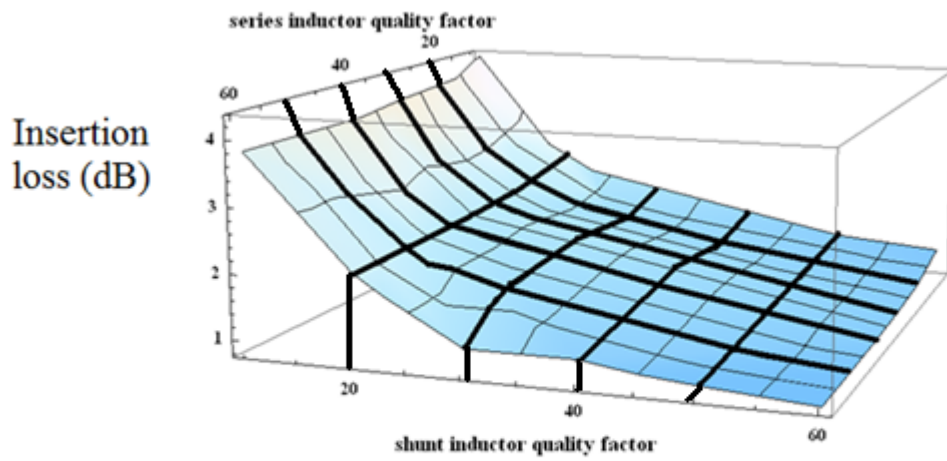


Fig.4

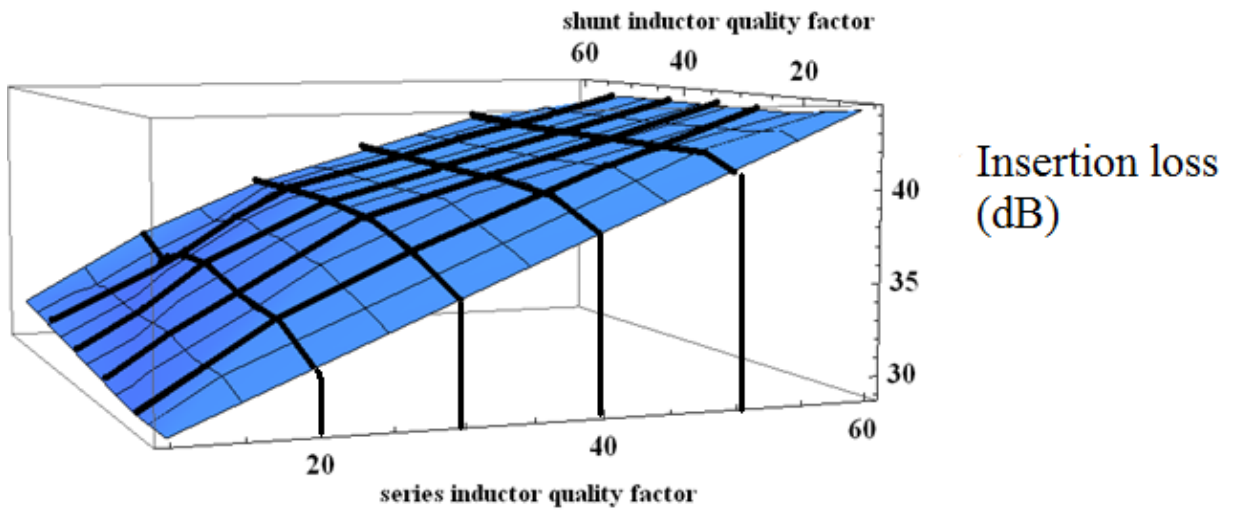


Fig5

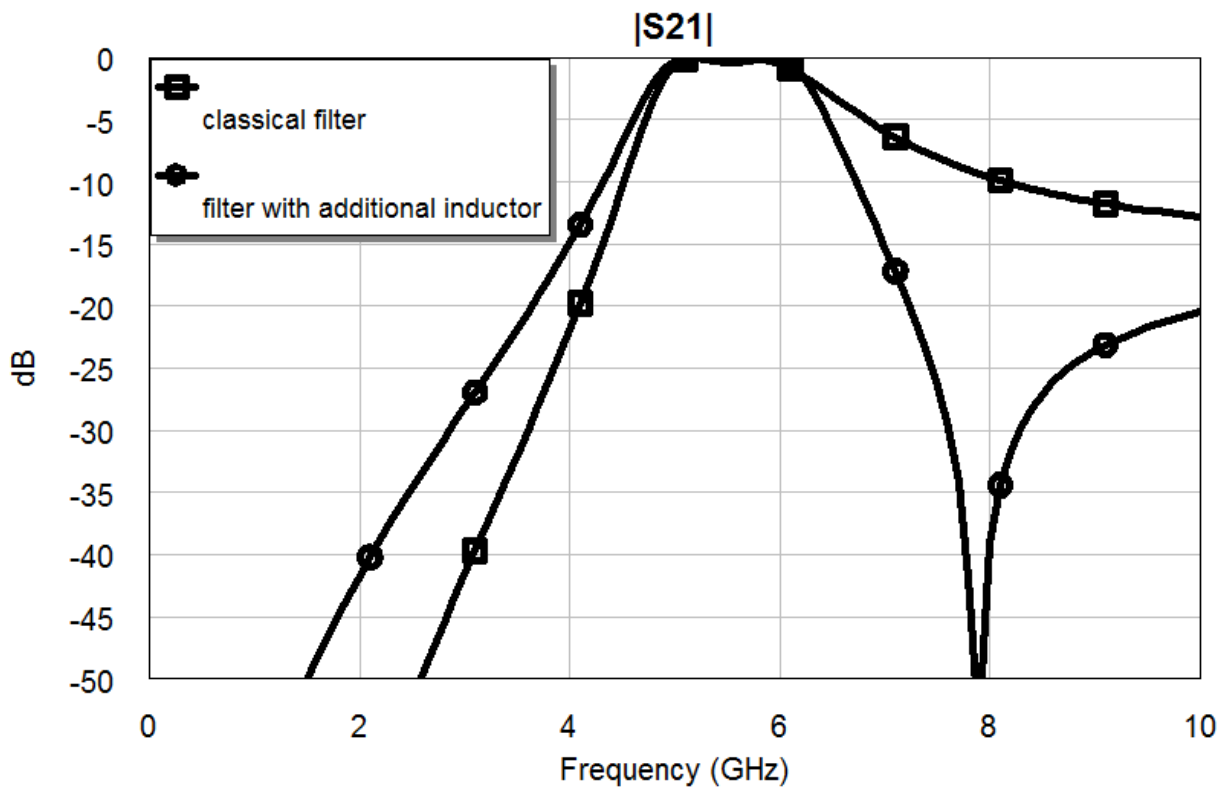


Fig.6

